Theory of excitonic high-order sideband generation in semiconductors under a strong terahertz field

Jie-Yun Yan*
Department of Physics, Tsinghua University, Beijing 100084, People's Republic of China
(Received 20 January 2008; published 20 August 2008)

We present the theory of excitonic high-order sideband generation (HSG) in semiconductors by an intense terahertz (THz) field. When the Coulomb interaction is neglected, we give an analytical solution to the HSG with the help of Floquet theory. Besides, the HSG is also studied by the quantum trajectory theory (saddle-point method) by which the HSG is explained by the interference of different quantum trajectories of excitons when accelerating in the external THz field. Both the exact analytic solution and the saddle-point method obtain consistent results: the spectrum of sidebands has an extended plateau where all the sidebands have almost the same intensity, which is similar to the high-order harmonic generation in atomic system. Moreover the HSG provides more flexibility in studying the quantum trajectory theory. When Coulomb interaction is considered, we find considerable Coulomb enhancement of HSG, which is absent in atomic system. The mechanism is discussed based on numerical calculations.

DOI: 10.1103/PhysRevB.78.075204 PACS number(s): 71.35.Cc, 78.20.Bh, 42.65.Ky

I. INTRODUCTION

The behavior of excitons under an ac electric field is an important issue in semiconductors. On one hand, excitons in semiconductors have the characteristics of atoms so that many similar effects have been "replicated" such as optical Stark effect[1,2] and exciton stabilization.[3] On the other hand, as exciton is a most fundamental quasiparticle in semiconductors when excited by lasers, its responses to the external optical field manifest the intrinsic many-body coherence such as the dynamical Franz-Keldysh effect[4] and the dynamic localization.[5,6] Now that the ac electric field can be realized by terahertz (THz) laser, excitons are expected to be controlled more easily by manipulating THz fields and hence have prosperous applications.

In semiconductors, one can create a hydrogen-atom-like exciton by a near infrared laser. Under the THz radiation, excitons absorb or emit different numbers of THz photons and generate sidebands to the near infrared excitation. We call this process as the excitonic high-order sideband generation (HSG).[7] The HSG in semiconductors has its counterpart in atom physics, i.e., the high-order harmonic generation (HHG),[8,9] which has been a major topic for decades with significant applications in attosecond physics[10] such as studying the time evolution of surface states using a pump-probe technique.[11–13]

However, there exists essential difference between the HHG in atomic physics and the HSG in semiconductors. The Coulomb interaction plays an important role in exciton system because the distance of each electron-hole pair in real space is within the power of Coulomb interaction after they are created from the vacuum state. In contrast, in the process of HHG, once an electron is excited out, it is free of the ion left behind and consequently the Coulomb interaction is negligible when driven by the electric field of the laser, which was proved theoretically.[9] Moreover, the HSG starts from the creation of elementary excitations in solids and hence has tunable excitation energy while the HHG involves atoms with fixed binding energy. Thus the THz-sideband spectroscopy is expected to provide more flexibility in studying the quantum trajectory, developed in atomic physics to understand the HHG. Recently, the quantum path interferences in HHG in argon have been observed experimentally.[14] We expect that the quantum path interference can be observed easily in semiconductors. Apart from a basic theoretical research, the HSG is also useful in many electro-optical applications such as wide-band optical multiplexers, optical pulses with ultrahigh repetition rate, and optical communication with THz bandwidth.

In the paper, we investigate HSG in semiconductors and get the consistent results by different methods. As we will show, the sidebands spectrum exhibits an extended plateau where all the sidebands have almost the same intensity. The results can be explained by the interference of different quantum trajectories based on a three-step model: (a) Excitons are created by the laser excitation. (b) Driven by the THz field, excitons accelerate along different quantum trajectories and acquire particular energies. (c) Excitons annihilate and generate sidebands contributed by different trajectories. When Coulomb interaction is considered, we find remarkable Coulomb enhancement effect in HSG, which is a characteristic different from HHG in atomic system. The mechanism of Coulomb enhancement effect is discussed based on numerical calculations in different excitation conditions.

The content of the paper is organized as follows: We first derive the analytic result of the HSG in the absence of Coulomb interaction in Sec. II. In Sec. III, the HSG is solved by saddle-point method. The results are discussed based on the quantum trajectory interference theory. In this section, the spectra calculated by the analytical method and saddle-point method are shown. The Coulomb enhancement effect is discussed in Sec. IV where the HSG is obtained by the space-time difference method and the conclusion is based on the numerical results under different excitation condition. Finally we present a brief summation. Some detailed derivations are appended for reference.

II. ANALYTIC SOLUTION

In this section, we give an analytic solution to the HSG without the Coulomb interaction considered. In semiconductors, a near infrared laser could excite electron-hole pairs and thus excitons are formed. The dynamics relating to behaviors of excitons are governed by the relative motion of electron-hole pairs. Thus the Hamiltonian could be written in momentum representation as

$$H = (k_x^2 + k_y^2 + k_z^2) + iF(t)\nabla_{k_z}, \tag{1}$$

where $F(t)$ is the electric field of THz laser $F(t)=F\cos(\omega t)$. $k_j(j=x,y,z)$ are the excitonic wave vectors in j direction. For convenience, we use the excitonic-Rydberg unit in the paper. The Hamiltonian is time periodic and can be treated in Floquet representation.[15] The quasienergies and quasienergy states read, respectively (see Appendix A)

$$\varepsilon_{km} = E_s(k) + \frac{F^2}{2\omega^2} + m\omega, \tag{2}$$

and

$$|q(t)\rangle = e^{im\omega t - 2ik_z\sqrt{2\gamma_0/\omega}\cos\omega t + i\gamma_0/2\sin 2\omega}|k\rangle, \tag{3}$$

where m is an integer, $E_s(k)=k^2$ is the energy of free exciton, and γ_0 is defined as $F^2/2\omega^3$.

Sideband generation is determined by the responding function

$$\chi(t,t') = \frac{i\theta(t-t')}{V}[\langle g|\mu K(t,t')\mu|g\rangle - \langle g|\mu K(t',t)\mu|g\rangle], \tag{4}$$

where $K(t,t')$ is the propagator of the system, V is the normalized volume, and θ is the step function. μ is the transition dipole. In the formula above, the first item in the bracket means a pair of electron hole is created at time t' by transition μ and evolves with the propagator $K(t,t')$ until time $t>t'$ when recombination happens with transition μ, and finally the system returns to ground state. In the recombination process, the excitonic sidebands are generated so the formula is just the description of HSG process. While the second item is nothing but a conjugate item of the first one in the bracket, we neglect it since then. The propagator is found to be

$$K(t,t') = |q(t)\rangle e^{-i(\epsilon_q - i\gamma_2)(t-t')}\langle q(t')|, \tag{5}$$

where γ_2 is the introduced dephasing rate. Therefore the linear corresponding function can be written as

$$\chi(t,t') = \frac{1}{V}\sum_{m,n}\frac{i}{\hbar}\theta(\tau)\mu_{qn+m}\mu_{qm}^* e^{-in\omega t - i\epsilon_{qm}\tau - \gamma_2\tau}, \tag{6}$$

where $\mu_{q,m} \equiv \frac{1}{T}\int_0^T \langle g|\mu|q(t')\rangle e^{im\omega t}dt'$ and $\tau \equiv t-t'$. It is easy to prove that the sideband spectrum $\chi(\Omega,\Omega')$ [Fourier transformation of $\chi(t,t')$] has the property

$$\chi(\Omega,\Omega') = 2\pi\delta(\Omega - \Omega' - n\omega)\chi_n(\Omega'), \tag{7}$$

where $\chi_n(\Omega')$ is a factor only determined by the excitation frequency Ω'. The property gives the characteristic of sideband spectrum: discreet and equidistant with an interval of a THz photon energy, which is the reflection of time periodicity in the system.

The dipole transition matrix element $\langle g|\mu|q(t)\rangle$ is (see Appendix B)

$$\langle g|\mu|q(t)\rangle = \frac{V\mu}{(2\pi)^3}\int e^{-2ik_z\sqrt{2\gamma_0/\omega}\cos\omega t + i\gamma_0/2\sin 2\omega t}d^3k, \tag{8}$$

and the responding function is consequently (see Appendix C)

$$\chi(t,t') = \theta(\tau)\frac{i\mu^2}{(2\pi)^3}\left(\sqrt{\frac{\pi}{i\tau}}\right)^3 e^{-i[F^2/2\omega^2 - i\gamma_2]\tau} \times e^{i4\gamma_0\sin^2\omega\tau/2/\omega\tau} i^{-n} e^{i2n\omega T^*} \times J_n\left(\frac{4\gamma_0\sin^2\frac{\omega\tau}{2}}{\omega\tau} - \gamma_0\sin\omega\tau\right), \tag{9}$$

with $T^* \equiv (t+t')/2$, $i^2=-1$, and $J_n(\cdots)$ is the n-order Bessel function of the first kind. With the Fourier transformation, we obtain the spectrum function as

$$\chi(\Omega,\Omega') \equiv \sum_n 2\pi\delta(\Omega - \Omega' - 2n\omega)\chi_{2n}(\Omega'), \tag{10}$$

where $\chi_{2n}(\Omega')$ is

$$\chi_{2n}(\Omega') = \mu^2\left(\frac{\omega}{4\pi}\right)^{3/2} e^{i(2n-1)\pi/4}\int d\tau e^{i[\Omega' + n\omega - F^2/2\omega^2 + i\gamma_2]\tau} \times \frac{1}{(\omega\tau)^{3/2}} e^{i4\gamma_0\sin^2\omega\tau/2/\omega\tau} J_n \times\left(\gamma_0\sin\omega\tau - \frac{4\gamma_0\sin^2\frac{\omega\tau}{2}}{\omega\tau}\right). \tag{11}$$

The odd order sidebands disappear due to the breakdown of symmetry in k_z space, as discussed in Appendix C. The $2N$th sideband strength is determined by $\chi_{2n}(\Omega')$. Notice that the $2N$th sideband is referred to the sideband with the frequency $\Omega + 2N\omega$.

III. QUANTUM TRAJECTORY INTERFERENCE

The excitonic motion in the THz field determines the sideband generation. From view of path integral, the excitons move along different trajectories when driven by the THz field. In this section, we get the HSG by the saddle-point method, which demonstrates the interference of different quantum trajectories. The Hamiltonian is transformed to

$$H(t) = (\boldsymbol{p} - \boldsymbol{A})^2, \tag{12}$$

where $\boldsymbol{p}$ is momentum vector and $\boldsymbol{A}$ is the vector potential $\boldsymbol{A}(t) = -\frac{F}{\omega}\sin(\omega t)\hat{e}_z$. The Schrodinger equation is

$$i\partial_t\psi(r,t) = H(t)\psi(r,t) + \boldsymbol{\mu}\cdot\boldsymbol{E}(t)\delta(r), \tag{13}$$

where $\boldsymbol{E}(t)$ is the excitation $\boldsymbol{E}(t)=\boldsymbol{E}_p\exp(-i\Omega t)+\text{c.c.}$, and $\boldsymbol{\mu}$ is the vector form of the dipole μ.

What we want to find is the polarization

$$\boldsymbol{P}(t) = i\int \boldsymbol{\mu}^* \delta(r) K(\boldsymbol{r}t,\boldsymbol{r}'t')\,\theta(t-t')\,\boldsymbol{\mu}\cdot\boldsymbol{E}(t')\,\delta(r')d\boldsymbol{r}d\boldsymbol{r}'dt', \tag{14}$$

where $K(rt,r't')$ is the propagator, which reads

$$K(\boldsymbol{r}t,\boldsymbol{r}'t') = \frac{1}{(2\pi)^3}\int d\boldsymbol{p}\, e^{i\boldsymbol{p}\cdot(\boldsymbol{r}-\boldsymbol{r}')-i\int_{t'}^{t}[\boldsymbol{p}-\boldsymbol{A}(t'')]^2 dt''}. \tag{15}$$

Substituting the propagator back and making the Fourier transformation, we can obtain the polarization

$$\boldsymbol{P}_{2N} \equiv \boldsymbol{P}(\Omega+2N\omega) = i\boldsymbol{\mu}^*\boldsymbol{\mu}\cdot\boldsymbol{E}_p\int e^{iS}\theta(\tau)dtd\tau\frac{d\boldsymbol{p}}{(2\pi)^3}, \tag{16}$$

where we extract out a most important quantity:

$$S(\boldsymbol{p},t,\tau) \equiv -\int_{t-\tau}^{t}[\boldsymbol{p}-\boldsymbol{A}(t'')]^2 dt'' + \Omega\tau + 2N\omega t. \tag{17}$$

Equation (16) has a clear physical meaning as a sum of probability amplitudes corresponding to the following processes: $\boldsymbol{\mu}\cdot\boldsymbol{E}_p$ represents the excitation of a pair of electron and hole by laser. The exciton propagates with the canonical momentum $\boldsymbol{p}$ under THz electric field for a period of time $\tau=t-t'$ then its wave function acquires a phase factor $e^{iS(\boldsymbol{p},t,\tau)}$ before the recombination of electron and hole by transition $\boldsymbol{\mu}^*$. (Here we neglect the dependence of dipole on the momentum.) The quantity $S(\boldsymbol{p},t,\tau)$ is just the quasiclassical action, describing the motion of exciton in the ac electric field with canonical momentum $\boldsymbol{p}$, which is a conversed quantity in this process.

The integral in Eq. (16) can be solved by saddle-point method, an approximation considering the dominating part coming from stationary points of the action. The stationary points are determined by the saddle-point equations $\partial_\nu S=0$ $(\nu=\boldsymbol{p},t,\tau)$, which read

$$\boldsymbol{p}\tau - \int_{t-\tau}^{t}\boldsymbol{A}(t')dt' = 0, \tag{18}$$

$$[\boldsymbol{p}-\boldsymbol{A}(t-\tau)]^2 = \Omega, \tag{19}$$

and

$$[\boldsymbol{p}-\boldsymbol{A}(t)]^2 - [\boldsymbol{p}-\boldsymbol{A}(t-\tau)]^2 = 2N\omega. \tag{20}$$

These equations have very nice physical meaning to the process of sibeband generation: As the velocity of the exciton under ac electric field is $\boldsymbol{p}-\boldsymbol{A}(t)$, Eq. (18) means the return of the electron to the position of the hole after acceleration by the electric field. While Eqs. (19) and (20) express the energy conservation of the excitation of *e-h* pair, and the energy conservation for the sideband generation through recombination of *e-h* pair, respectively.

By solving these saddle-point equations, we can find the relating saddle points τ_n and t_n. The action is then

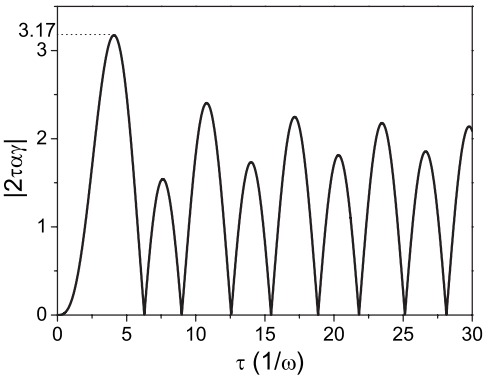

FIG. 1. The function of $|2\tau\alpha\gamma|$ as a function of the return time τ.

$$S(t,\tau) = 2N\omega t + (\Omega-U_p)\tau + U_p\tau\alpha\gamma\cos(2\omega t-\omega\tau) + U_p\tau\gamma^2, \tag{21}$$

where

$$U_p \equiv \frac{F^2}{2\omega^2}, \quad \alpha \equiv \cos\frac{\omega\tau}{2} - \frac{\sin\frac{\omega\tau}{2}}{\frac{\omega\tau}{2}}, \quad \beta \equiv \sin\frac{\omega\tau}{2},$$

$$\text{and} \quad \gamma \equiv \frac{\sin\frac{\omega\tau}{2}}{\frac{\omega\tau}{2}}.$$

The action can give us some insight on the sideband generation result. As it describes the motion of exciton under the electric field from which the exciton gets the energy increment to generate sidebands when in recombination, it is obvious that the $2\tau\alpha\gamma$ determines the variation of S_{cl} as a function of time and therefore determines the maximum energy it can get from the electric field. It should note that $2\tau\alpha\gamma$ has a maximum of 3.17, as shown in Fig. 1. Consequently we can get that the maximum sideband number $(2N)$ lies about $3.17U_p-\Omega/\omega$, which will be checked out later.

The strength of sidebands is finally obtained as

$$\boldsymbol{P}_{2N} = \sum_n \frac{i\mu^2\boldsymbol{E}_p e^{iS(t_n,\tau_n)}}{(\sqrt{4\pi\tau_n i}+0^+)^3}\sqrt{\frac{2\pi^2 i^2}{\det S''}}, \tag{22}$$

where t_n,τ_n are the saddle points for t,τ and the summation runs over all corresponding saddle points. The infinitesimal 0^+ comes from the regularized Gaussian integration over $\boldsymbol{p}$. S'' represents the second-order derivative Jacobian determinant of the corresponding action:

$$S'' = \begin{vmatrix} \frac{\partial^2 S(t,\tau)}{\partial t^2} & \frac{\partial^2 S(t,\tau)}{\partial t\,\partial\tau} \\ \frac{\partial^2 S(t,\tau)}{\partial t\,\partial\tau} & \frac{\partial^2 S(t,\tau)}{\partial\tau^2} \end{vmatrix}. \tag{23}$$

The HSG is then determined by $\chi_{2n}=|\boldsymbol{P}_{2N}/\boldsymbol{E}_p|$.

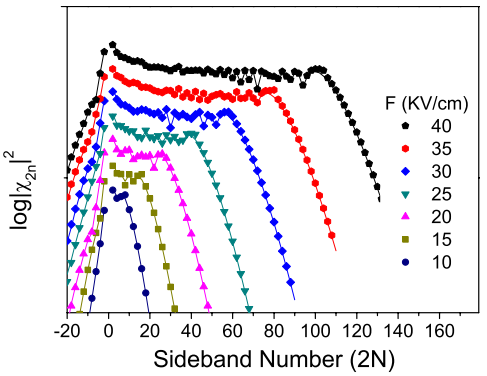

FIG. 2. (Color online) The sideband strength calculated by saddle-point method (symbols) and analytically (lines) with different electric-field strength F. Results given by these two methods for a certain value of F are plotted with the same colors. Results with different F are shifted vertically for clarity. The frequency of excitation is set as $\Omega=-8$ meV. THz photon energy is 5 meV.

The results calculated by saddle-point method are shown in Figs. 2 and 3. The excitonic-Rydberg energy is set as 5 meV and the Bohr radius is 10 nm. The frequency of the ac electric field is 5 meV. In Fig. 2, the THz field strength is changed from 10 to 40 KV/cm by steps of 5 KV/cm with the frequency of excitation fixed to $\Omega=-8$ meV (since the band gap is set to zero, the frequency of the excitation is given relative to the band gap). In Fig. 3, the frequency of excitation is changed with four different values: −8, −18, −28, and −38 meV with the THz field strength fixed to 30 KV/cm. All the spectra have the same characteristic: it falls off for the first few sidebands, then exhibits a plateau where all sidebands have almost the same strength, and ends up with a sharp cutoff. The cut-off position is consistent with the analysis before.

Actually the sideband strength given above is the quantum interference results of all different trajectories. As mentioned above, the final result should sum over all the saddle points. For variable τ, every saddle point τ_n represents the time from excitation to recombination and so represents a

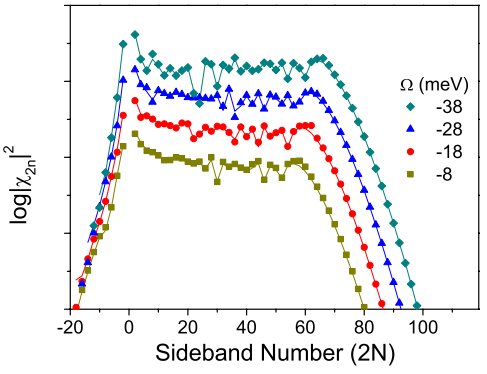

FIG. 3. (Color online) The sideband strength calculated by saddle-point method (symbols) and analytically (lines) with different excitations Ω. The results given by these two methods for a certain value of Ω are plotted with the same colors. Results with different Ω are shifted vertically for clarity. The strength of the THz field is fixed to 30 KV/cm. THz photon energy is 5 meV.

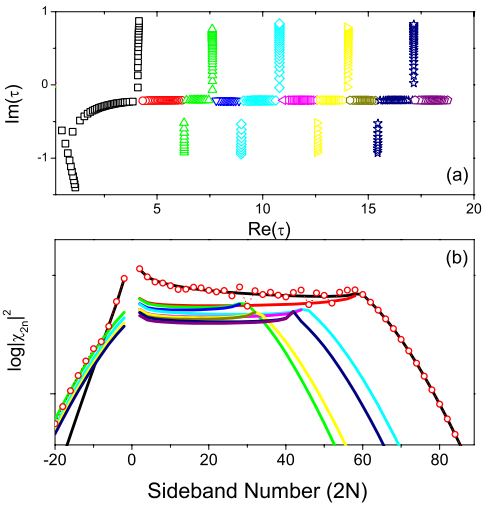

FIG. 4. (Color online) The interference of different quantum trajectories. (a) The distribution of saddle points of τ_n. Only those relating to the first ten trajectories are given. Different trajectories are classified by different symbols (colors). (b) The sideband strength is generated by these ten trajectories, expressed with different color lines correspondingly. The interference result is plotted with hollow circle line. The excitonic-Rydberg unit is used for τ and χ_{2n}.

quantum trajectory. The time periodicity of the electric field leads to the infinitude of τ_n while the contribution coming from τ_n with large real part is less important. We use the following parameters to discuss the interference of quantum trajectories: the electric-field strength is 30 KV/cm with frequency of 5 meV and excitation Ω of −8 meV. We only give saddle points of first ten trajectories shown with different symbols (colors) in Fig. 4(a). The sidebands generated by these ten trajectories are plotted in Fig. 4(b) where the result of interference is also shown. It is obvious that the interference result of these ten trajectories is enough to get the accurate result. Among these trajectories the first trajectories (the saddle point of τ with the least real part) has the largest contribution to the sideband strength so that it almost determines the final result.

IV. COULOMB ENHANCEMENT EFFECT

As mentioned in Sec. I, the Coulomb interaction plays an important role when excitons accelerate in the THz field. In this section, we will discuss the effect of Coulomb interaction. The HSG is based on the equation of motion in real space

$$i\partial_t\psi(\rho,z,t) = H(t)\psi(\rho,z,t) + \boldsymbol{\mu}\cdot\boldsymbol{E}(t)\delta(z)\frac{\delta(\rho)}{2\pi\rho}, \qquad (24)$$

and

$$H = -(\nabla_\rho^2 + \nabla_z^2) + F(t)z - \frac{2}{\sqrt{\rho^2+z^2}}, \qquad (25)$$

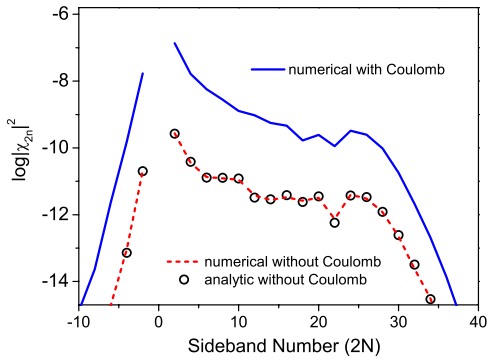

FIG. 5. (Color online) The sideband strength calculated by finite difference method with (solid line) and without (dashed line) Coulomb interaction. Also the analytic result without Coulomb interaction (hollow circle symbols) is given for reference. The strength of THz field is 20 KV/cm and the frequency of excitation is $\Omega=-8$ meV. Other parameters are the same to those used in Fig. 2 except that the dephasing factor is set to 0.5 meV. The excitonic-Rydberg unit is used for χ_{2n}.

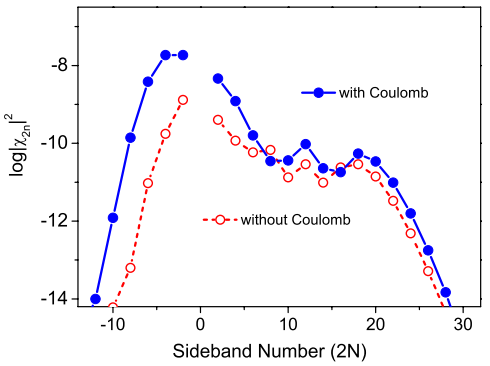

FIG. 6. (Color online) The sideband strength calculated by finite difference method with (solid line) and without (dashed line) the Coulomb interaction. The strength of THz field is 20 KV/cm and the excitation energy is $\Omega=18$ meV. Other parameters are the same to those used in Fig. 5. The excitonic-Rydberg unit is used for χ_{2n}.

where ρ and z are the relative coordinates of the electron and hole in the $x-y$ plane and z direction. We can get the sideband spectrum by finite difference method.[16]

Figure 5 shows the results calculated with finite difference method with and without Coulomb interaction. The analytic result is also plotted to testify the validity of numerical method. The strength and frequency of the electric field are 20 KV/cm and 5 meV, respectively. The excitation is $\Omega=-8$ meV and the dephasing factor of wave function is set to 0.5 meV. Without Coulomb interaction, the numerical result accords well with the analytic one, which proves the validity of the numerical method. With Coulomb interaction, the sideband generation strength is enhanced with several orders of magnitude while there is no significant difference in the characteristics of the sideband such as the plateau and the cut-off position. As discussed in Sec. I, it is the peculiar characteristic of the exciton in semiconductors. Because the Coulomb interaction cannot provide extra power, the unchanging of the cut-off position is understandable while which sidebands are enhanced more lies on the value of excitation energy. In Fig. 5, the energy of near infrared laser is below the gap of exciton continuum; therefore the excitation is a kind of virtual process in the absence of Coulomb interaction. After the Coulomb interaction is considered, the process turns from virtual process to real one because the density of states below the band edge is increased significantly due to separated excitonic states. The change of state density can significantly improve the probability of excitation so that the strength of sideband generation is enhanced considerably.

If we use the near infrared laser with energy above the band gap of exciton such as $\Omega=18$ meV, the influence of Coulomb enhancement for most sideband $N>0$ is not expected so obviously because the excitation is always a real physical process with or without Coulomb interaction, which can be seen from Fig. 6. Interestingly, the obvious enhancement is still observed for sideband $N<0$. The reason is that, although the excitation is a real process in this case, the combination is a virtual one without Coulomb interaction. Coulomb interaction will turn the combination process to a real one then the strength of sideband generation is improved significantly, which proves our explanation from another side.

V. CONCLUSION

The HSG under an intense THz field in semiconductors is investigated both analytically and numerically. Besides an exact analytic solution, we get the spectrum of HSG by the saddle-point method by which we present an explicit physical interpretation to the HSG by the interference of quantum trajectories. In contrast with HHG in atom system, the HSG of exciton in semiconductors has more flexibility in studying the quantum trajectory such as the tunable excitation. Moreover, the considerable Coulomb enhancement effect is found in exciton system. This enhancement due to the Coulomb interaction can be explained by the transition between virtual processes and real processes when excitonic creation or recombination happens. The discussion is supported by the numerical results.

ACKNOWLEDGMENTS

The author would like to acknowledge Bang-fen Zhu and Ren-Bao Liu for stimulating discussions. This work was supported by the Natural Science Foundation of China (Grant Nos. 10334040, 10574076, and 10774086), and by the Program of Basic Research Development of China (Grant No. 2006CB921500).

APPENDIX A: FLOQUET REPRESENTATION

If the system is time periodic, i.e., the Hamiltonian satisfies

$$H(t+T)=H(t), \tag{A1}$$

where $T=2\pi/\omega$, then the wave function can be written as

$$|\psi\rangle = e^{-i(\epsilon_q + m\omega)t}|q(t)\rangle, \tag{A2}$$

where m is an integer and $|q(t)\rangle$ is quasienergy wave function, satisfying the equation

$$(H - i\partial_t)|q(t)\rangle = (\epsilon_q + m\omega)|q(t)\rangle. \tag{A3}$$

With a gauge transformation, the Hamiltonian $H=k^2 \equiv E(k)$ has the free particle form and the wave vector becomes

$$\tilde{k} = \left(k_x, k_y, k_z - \frac{F}{\omega}\sin\,\omega t\right). \tag{A4}$$

The quasienergy and quasienergy state are[17]

$$\varepsilon_{km} \equiv m\omega + \frac{1}{T}\int_0^T E(\tilde{k})dt', \tag{A5}$$

and

$$|q(t)\rangle \equiv \exp\left[im\omega t + i\epsilon_q t - i\int_0^t \epsilon(\tilde{k})dt'\right]|k\rangle. \tag{A6}$$

Therefore, we can get the quasienergy

$$\epsilon_{km} = E(k) + \frac{F^2}{2\omega^2} + m\omega, \tag{A7}$$

and hence the quasienergy states

$$|q(t)\rangle = e^{im\omega t - 2ik_z\sqrt{2\gamma_0/\omega}\,\cos\,\omega t + i\gamma_0/2\,\sin\,2\omega t}|k\rangle, \tag{A8}$$

where γ_0 is $F^2/2\omega^3$.

APPENDIX B: DIPOLE TRANSITION MATRIX ELEMENT

The dipole transition matrix element can be expressed as

$$\langle g|\mu|q(t)\rangle = \sum_m e^{im\omega t}\mu_{q,m}, \tag{B1}$$

where $\mu_{q,m}$ is defined as

$$\mu_{q,m} \equiv \frac{1}{T}\int_0^T \langle g|\mu|q(t')\rangle e^{im\omega t}dt'. \tag{B2}$$

Expanding the quasienergy state in momentum space, the dipole transition matrix can be further written as

$$\langle g|\mu|q(t)\rangle = \frac{V}{(2\pi)^3}\int d^3k \sum_m e^{-im\omega t}\mu\mu_{q,km}, \tag{B3}$$

where $\mu_{q,km}$ is defined as

$$\mu_{q,km} \equiv \frac{1}{T}\int_0^T \langle g|x=0|k,m\rangle dt'. \tag{B4}$$

With the k dependence of the dipole matrix element neglected, the dipole matrix element of the Floquet state is[18]

$$\mu_{q,km} = \mu i^{-m} J_m\left(2k_z\sqrt{\frac{2\gamma_0}{\omega}}, \frac{i\gamma_0}{2}\right), \tag{B5}$$

where the Bessel function is defined as

$$J(\alpha,\beta) = \frac{i^m}{2\pi}\int_{-\pi}^{+\pi} d\phi\,\exp[im\phi - i\alpha\,\cos\,\phi + i\beta\,\sin\,2\phi]. \tag{B6}$$

Therefore the dipole transition matrix element is

$$\langle g|\mu|q(t)\rangle = \frac{V\mu}{(2\pi)^3}\int e^{-2ik_z\sqrt{2\gamma_0/\omega}\,\cos\,\omega t + i\gamma_0/2\,\sin\,2\omega t}d^3k. \tag{B7}$$

APPENDIX C: RESPONDING FUNCTION

Since the dipole transition matrix element is obtained, the responding function is then

$$\chi(t,t') = \frac{i}{\hbar}\theta(\tau)\frac{\mu^2}{(2\pi)^3}e^{-i[F^2/2\omega^2 - i\gamma_2]\tau}\int d^3k e^{-ik^2\tau} \times e^{4ik_z\sqrt{2\gamma_0/\omega}\,\sin\,\omega\tau/2\,\sin\,\omega T^*}e^{(i\gamma_0\,\sin\,\omega\tau\,\cos\,2\omega T^*)}, \tag{C1}$$

where $T^* \equiv (t+t')/2$. The above integration over k_x and k_y is easy to get. Using the properties of Bessel function, the responding function becomes

$$\chi(t,t') = \frac{i}{\hbar}\theta(\tau)\frac{\mu^2}{(2\pi)^3}e^{-i[F^2/2\omega^2 - i\gamma_2]\tau}\left(\sqrt{\frac{\pi}{i\tau}}\right)^2\sum_n i^{-n} \times J_n(-\gamma_0\,\sin\,\omega\tau)e^{i2n\omega T^*} \times 2\int_0^{+\infty} dk_z e^{-ik_z^2\tau}\sum_m \times J_{2m}\left(4ik_z\sqrt{\frac{2\gamma_0}{\omega}}\sin\frac{\omega\tau}{2}\right)e^{i2m\omega T^*}. \tag{C2}$$

As for the integration over k_z, it is important to notice that the integration is zero for odd order Bessel function in the integrand because of the asymmetry in k_z space, which leads to the vanishing of odd order sidebands, as shown later. The breaking down of space symmetry in field direction is also the main effect caused by THz field, in addition to the time periodicity. After solving the integration,[19] we can get the responding function as

$$\chi(t,t') = \frac{i}{\hbar}\theta(\tau)\frac{\mu^2 i^{-n}}{(2\pi)^3}\left(\sqrt{\frac{\pi}{i\tau}}\right)^3 \times e^{-i[F^2/2\omega^2 - i\gamma_2]\tau}e^{i4\gamma_0\,\sin^2\,\omega\tau/2/\omega\tau} \times e^{i2n\omega T^*}J_n\left(\frac{4\gamma_0\,\sin^2\frac{\omega\tau}{2}}{\omega\tau} - \gamma_0\,\sin\,\omega\tau\right). \tag{C3}$$

With Fourier transformation, we get the spectrum function as

$$\chi(\Omega,\Omega') \equiv \sum_n 2\pi\delta(\Omega - \Omega' - 2n\omega)\chi_{2n}(\Omega'), \tag{C4}$$

where $\chi_{2n}(\Omega')$ is given by Eq. (11).

*yanjy03@mails.thu.edu.cn

[1] D. Fröhlich, A. Nöthe, and K. Reimann, Phys. Rev. Lett. **55**, 1335 (1985).
[2] S. G. Carter, V. Birkedal, C. S. Wang, L. A. Coldren, A. V. Maslov, D. S. Citrin, and M. S. Sherwin, Science **310**, 651 (2005).
[3] R.-B. Liu and B.-F. Zhu, Phys. Rev. B **66**, 033106 (2002).
[4] A. P. Jauho and K. Johnsen, Phys. Rev. Lett. **76**, 4576 (1996).
[5] D. H. Dunlap and V. M. Kenkre, Phys. Rev. B **34**, 3625 (1986).
[6] K. W. Madison, M. C. Fischer, R. B. Diener, Q. Niu, and M. G. Raizen, Phys. Rev. Lett. **81**, 5093 (1998).
[7] R.-B. Liu and B.-F. Zhu, in *Physics of Semiconductors: 28th International Conference on the Physics of Semiconductors–ICPS 2006*, AIP Conf. Proc. No. 893 (AIP, New York, 2007), p. 1455.
[8] P. B. Corkum, Phys. Rev. Lett. **71**, 1994 (1993).
[9] M. Lewenstein, Ph. Balcou, M. Yu. Ivanov, A. L'Huillier, and P. B. Corkum, Phys. Rev. A **49**, 2117 (1994).
[10] P. Agostini and L. F. DiMauro, Rep. Prog. Phys. **67**, 813 (2004).
[11] A. L'Huilliera, D. Descampsb, A. Johansson, J. Norin, J. Mauritsson, and C.-G. Wahlstr, Eur. Phys. J. D **26**, 91 (2003).
[12] M. Hentschel, R. Kienberger, C. Spielmann, G. A. Reider, N. Milosevic, T. Brabec, P. Corkum, U. Heinzmann, M. Drescher, and F. Krausz, Nature (London) **414**, 509 (2001).
[13] M. Drescher, M. Hentschel, R. Kienberger, and M. Uiberacker, Nature (London) **419**, 803 (2002).
[14] A. Zaïr, M. Holler, A. Guandalini, F. Schapper, J. Biegert, L. Gallmann, U. Keller, A. S. Wyatt, A. Monmayrant, I. A. Walmsley, E. Cormier, T. Auguste, J. P. Caumes, and P. Saliéres, Phys. Rev. Lett. **100**, 143902 (2008).
[15] R. B. Liu and B. F. Zhu, J. Phys.: Condens. Matter **12**, L741 (2000).
[16] S. Glutsch, D. S. Chemla, and F. Bechstedt, Phys. Rev. B **54**, 11592 (1996).
[17] W. A. Houston, Phys. Rev. **57**, 184 (1940).
[18] Howard R. Reiss, Phys. Rev. A **22**, 1786 (1980).
[19] I. S. Gradshteyn and K. M. Ryzhik, *Tables of Integrals, Series, and Products* (Academic, New York, 1980).